Computational Materials Science 118 (2016) 259–268

Contents lists available at ScienceDirect

Computational Materials Science

journal homepage: www.elsevier.com/locate/commatsci

# A QM/MM approach for low-symmetry defects in metals

Liam Huber [a,*], Blazej Grabowski [b], Matthias Militzer [c], Jörg Neugebauer [b], Jörg Rottler [a]

[a] Department of Physics and Astronomy, The University of British Columbia, 6224 Agricultural Rd., Vancouver, BC V6T 1Z1, Canada
[b] Max-Planck-Institut für Eisenforschung GmbH, D-40237 Düsseldorf, Germany
[c] Centre for Metallurgical Process Engineering, The University of British Columbia, 309-6350 Stores Road, Vancouver, BC V6T 1Z4, Canada

ARTICLE INFO

*Article history:*
Received 11 November 2015
Received in revised form 15 February 2016
Accepted 21 March 2016
Available online 31 March 2016

*Keywords:*
*Ab initio* modeling
Multiscale modeling
Interfaces
Solutes

ABSTRACT

Concurrent multiscale coupling is a powerful tool for obtaining quantum mechanically (QM) accurate material behavior in a small domain while still capturing long range stress fields using a molecular mechanical (MM) description. We outline an improved scheme for QM/MM coupling in metals which permits the QM treatment of a small region chosen from a large, arbitrary MM domain to calculate total system energy and relaxed geometry. In order to test our improved method, we compute solute–vacancy binding in bulk Al as well as the binding of Mg and Pb to a symmetric Σ5 grain boundary. Results are calculated with and without our improvement to the QM/MM scheme and compared to periodic QM results for the same systems. We find that our scheme accurately and efficiently reproduces periodic QM target values in these test systems and therefore can be expected to perform well using more general geometries.



## 1. Introduction

Quantum mechanical (QM) calculations provide access to a large number of material parameters and atomistic details. As computational power continues to increase, more and more complex situations can be studied. However, even with very efficient QM methods such as the Kohn–Sham (KS) density functional theory (DFT) and the use of pseudopotentials (PPs), structural optimization is still limited to a few hundreds of atoms. While DFT captures the electronic and magnetic details with high accuracy, the constraints on system size prevent the representation of many interesting geometries and can cause inaccuracies in energies and forces due to mistreatment of long-range strain effects.

In contrast to QM calculations, molecular mechanical (MM) calculations relying on classical atomic interactions can easily treat systems of millions of atoms. However, common many-body potentials for metals like those constructed using the embedded atom method (EAM) are unable to capture all of the complexity that is found during electronic QM calculations. Even more importantly, the generation of these high-quality potentials is itself very time consuming and not straightforward. In the case of alloys, separate potentials must be generated for each interaction between species of atoms. This is particularly limiting in computationally aided alloy design, where it is often necessary to scan through many different alloying elements to search for trends in properties that act as indicators for macroscopic material behavior.

Atomistic QM/MM schemes attempt to obtain the best of both of these techniques by partitioning a large system into two domains and treating a small domain of particular interest (e.g. a crack tip, dislocation, or solute) with QM accuracy, while concurrently coupling this small subsection to a much larger domain where a MM treatment is sufficient [1–5]. Such methods harness the power of QM calculations for chemical interactions while relying on efficient MM techniques to capture long-range elastic behavior. The region of interest could also be coupled to a continuum description of the larger system [6–12], but here we focus on coupling exclusively to a classical atomistic representation.

QM/MM methods are particularly sensitive to how the partitioning of the system and the interaction between the different domains is handled. For molecular systems, electrons are well localized in bonds, and there are mature methods in the vein of the ONIOM [13–15] scheme (implemented in the GAUSSIAN code package,) which partition the system by cutting the bonds and saturating them with "link atoms". For metals, the delocalized nature of the electrons makes this a poor approximation, and a different partitioning scheme must be used. While not as well established as molecular QM/MM, atomistic QM/MM for metals have seen important developments in recent years [1–5].

Since the atoms in the QM domain for a QM/MM calculation do not necessarily repeat periodically inside reasonably sized boundaries, atomistic QM/MM calculations frequently use vacuum

* Corresponding author.
*E-mail address:* huberl@phas.ubc.ca (L. Huber).

http://dx.doi.org/10.1016/j.commatsci.2016.03.028
0927-0256/

clusters for the QM component calculations. The resulting vacuum surfaces interfere with the perception of the QM domain of being embedded in a much larger MM region. To mitigate this effect, Liu et al. [3] introduced a set of boundary—or buffer—atoms, which, while present in the QM calculation, draw their relaxation forces from the MM calculation. Although this is a distinct improvement, the strong electronic perturbations created by the vacuum surface penetrate deeply, and very large buffer regions are needed to isolate the QM core from the vacuum surface. Recently, in an effort to resolve this problem, Zhang et al. [5] suggested a method in which the KS DFT Hamiltonian is modified by the addition of a term which penalizes charge densities that deviate from a target density. By using a bulk-like charge density as a target and giving the penalty term a spatial dependence so that it is fully active only near the outer edge of the QM domain, the presence of the vacuum surface is masked. The problem of vacuum surfaces was also addressed by Woodward and Rao [6] in the context of coupling QM to a lattice Green's function (LGF) solution. They eliminate the vacuum by extending the domain of atoms treated by the LGF right to the edges of the QM simulation cell. However, QM/LGF coupling is not straightforward when grain boundaries pass through the coupling domain [7]. Moreover, by using EAM potentials instead of LGFs we can account for nonlinear deformations.

In this paper, we propose an improved method in the context of existing atomistic QM/MM schemes. In a similar vein as Woodward and Rao, we eliminate the vacuum surfaces with the introduction of extra material. Unlike Woodward and Rao, the atoms we introduce are not part of the system being relaxed. Replacing the vacuum surface with a material–material interface reduces the electronic contrast at the edges of the QM domain, consequently improving the quality of QM forces and energies. We implement the method using KS DFT and molecular statics to calculate solute–vacancy binding in bulk Al, and solute–grain boundary (GB) binding at a symmetric $\Sigma5(120)[001]53.1^\circ$ tilt GB in Al for the solutes Mg and Pb. These systems were chosen so that they can also be studied using regular periodic DFT, which serves as a benchmark for the QM/MM method. Sources of error in the multiscale scheme are evaluated critically, and the performance of our improved method is assessed by the accuracy of binding energies obtained.

## 2. Method

### 2.1. Theory

Consider the decomposition of a very large system into two regions: a small region (I) of great interest that we would like to treat with QM accuracy, and a much larger region (II) for which a simpler classical MM representation will suffice. As in Refs. [16,8], we can decompose the total energy of this system as

$$E_{\mathrm{I+II}} = E_{\mathrm{I}}^{\mathrm{QM}} + E_{\mathrm{II}}^{\mathrm{MM}} + E_{\mathrm{int}}, \tag{1}$$

where subscripts indicate the region of the system or the interaction introduced by the decomposition, and superscripts QM and MM indicate association of the energy with a quantum or classical representation, respectively. This ideal decomposition is shown schematically in Fig. 1(a). The description of the interaction energy, $E_{\mathrm{int}}$, between the two regions will define the flavor of the coupling scheme. Following the work of Choly et al. [1], we choose a classical approximation of $E_{\mathrm{int}}$:

$$E_{\mathrm{int}} \approx E_{\mathrm{int}}^{\mathrm{MM}} = E_{\mathrm{I+II}}^{\mathrm{MM}} - E_{\mathrm{I}}^{\mathrm{MM}} - E_{\mathrm{II}}^{\mathrm{MM}}. \tag{2}$$

Substituting this approximation back into Eq. (1), we obtain the QM/MM coupled energy, $E_{\mathrm{I+II}}^{\mathrm{QM/MM}}$, as

$$E_{\mathrm{I+II}} \approx E_{\mathrm{I+II}}^{\mathrm{QM/MM}} = E_{\mathrm{I+II}}^{\mathrm{MM}} + E_{\mathrm{I}}^{\mathrm{QM}} - E_{\mathrm{I}}^{\mathrm{MM}}. \tag{3}$$

Calculations in this representation involve a single MM calculation of the entire large system, and two vacuum cluster calculations of the smaller region I with QM and MM, respectively. This is shown schematically in Fig. 1(b), where we have followed the work of Liu et al. [3] and introduced the labels, "core" and "buffer", to subdivide region I into two zones. In the core, the energetic contributions from the MM representations of region I and region I + II cancel out, and we are left with a QM contribution to the total energy. In the buffer, we would hope that the energy contributions from the QM and MM representations of the buffer-vacuum surface also cancel, but this can in general not be expected. This poor cancellation between QM and MM representations in the buffer zone is a direct result of the interaction energy approximation in Eq. (2). However, when considering energy differences between two systems, one may expect an increasing amount of error cancellation depending on the degree of similarity of the buffer zone geometries.

In addition to the energetics of our coupled system, we are also interested in obtaining accurately relaxed structures. To calculate atomic forces, we take derivatives of $E_{\mathrm{I+II}}^{\mathrm{QM/MM}}$ from Eq. (3) with respect to atomic positions, $\mathbf{R}$. For atoms in region II, atomic forces are very simple since these atoms are only represented in the MM calculation of the entire region I + II,

$$\mathbf{F}_{\mathrm{I+II}}^{\mathrm{QM/MM}}(\mathbf{R} \in \mathrm{II}) = -\nabla_{\mathbf{R}\in\mathrm{II}} E_{\mathrm{I+II}}^{\mathrm{QM/MM}} = -\nabla_{\mathbf{R}\in\mathrm{II}} E_{\mathrm{I+II}}^{\mathrm{MM}} = \mathbf{F}_{\mathrm{I+II}}^{\mathrm{MM}}(\mathbf{R} \in \mathrm{II}). \tag{4}$$

When calculating forces on atoms in the core of region I, there are contributions from all three components:

$$-\nabla_{\mathbf{R}\in\mathrm{I_{core}}} E_{\mathrm{I+II}}^{\mathrm{QM/MM}} = \mathbf{F}_{\mathrm{I+II}}^{\mathrm{MM}}(\mathbf{R} \in \mathrm{I_{core}}) + \mathbf{F}_{\mathrm{I}}^{\mathrm{QM}}(\mathbf{R} \in \mathrm{I_{core}}) - \mathbf{F}_{\mathrm{I}}^{\mathrm{MM}}(\mathbf{R} \in \mathrm{I_{core}}). \tag{5}$$

If the thickness of the buffer zone is greater than the MM potential's cutoff radius, then the two MM forces above are identical and cancel perfectly. Even when the buffer thickness is slightly less than the cutoff distance, the difference between $\mathbf{F}_{\mathrm{I+II}}^{\mathrm{MM}}(\mathbf{R} \in \mathrm{I_{core}})$ and $\mathbf{F}_{\mathrm{I}}^{\mathrm{MM}}(\mathbf{R} \in \mathrm{I_{core}})$ is small since the potential must go to zero near the cutoff. To ensure that the net forces in the core of region I come from the QM calculation, we introduce a correction force

$$\mathbf{F}_{\mathrm{I_{core}}}^{\mathrm{corr}}(\mathbf{R} \in \mathrm{I_{core}}) = -\mathbf{F}_{\mathrm{I+II}}^{\mathrm{MM}}(\mathbf{R} \in \mathrm{I_{core}}) + \mathbf{F}_{\mathrm{I}}^{\mathrm{MM}}(\mathbf{R} \in \mathrm{I_{core}}), \tag{6}$$

such that the forces in the region I core are purely QM,

$$\mathbf{F}_{\mathrm{I+II}}^{\mathrm{QM/MM}}(\mathbf{R} \in \mathrm{I_{core}}) = \mathbf{F}_{\mathrm{I}}^{\mathrm{QM}}(\mathbf{R} \in \mathrm{I_{core}}). \tag{7}$$

We follow a similar approach in the buffer of region I, where we have

$$-\nabla_{\mathbf{R}\in\mathrm{I_{buff}}} E_{\mathrm{I+II}}^{\mathrm{QM/MM}} = \mathbf{F}_{\mathrm{I+II}}^{\mathrm{MM}}(\mathbf{R} \in \mathrm{I_{buff}}) + \mathbf{F}_{\mathrm{I}}^{\mathrm{QM}}(\mathbf{R} \in \mathrm{I_{buff}}) - \mathbf{F}_{\mathrm{I}}^{\mathrm{MM}}(\mathbf{R} \in \mathrm{I_{buff}}). \tag{8}$$

Since forces $\mathbf{F}_{\mathrm{I+II}}^{\mathrm{MM}}(\mathbf{R} \in \mathrm{I_{buff}})$ are drawn from an MM calculation of the entire system, these forces are the MM representation of the true forces on buffer atoms. Their quality is tied to the quality of the MM potential itself, which can be expected to represent the long range elastic behavior well. Both $\mathbf{F}_{\mathrm{I}}^{\mathrm{QM}}(\mathbf{R} \in \mathrm{I_{buff}})$ and $\mathbf{F}_{\mathrm{I}}^{\mathrm{MM}}(\mathbf{R} \in \mathrm{I_{buff}})$, however, are strongly influenced by their vacuum surfaces. Since these surfaces are artifacts of our decomposition and do no exist in the true system, these forces are *not* physically reasonable. While these terms enter with opposite signs, there is, unfortunately, no guarantee that the MM and QM forces in the buffer will cancel well. This observation can be found in Ref. [3] and we follow their proposed solution to apply another correction force to atoms in the buffer region:

$$\mathbf{F}_{\mathrm{I_{buff}}}^{\mathrm{corr}}(\mathbf{R} \in \mathrm{I_{buff}}) = -\mathbf{F}_{\mathrm{I}}^{\mathrm{QM}}(\mathbf{R} \in \mathrm{I_{buff}}) + \mathbf{F}_{\mathrm{I}}^{\mathrm{MM}}(\mathbf{R} \in \mathrm{I_{buff}}). \tag{9}$$

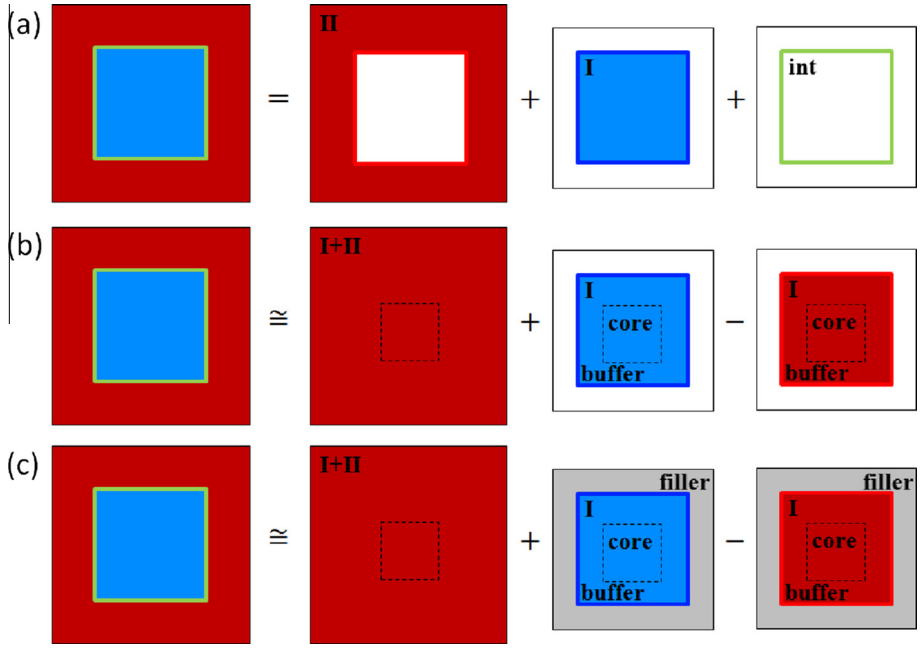


**Fig. 1.** Schematic of the system partitioning into (a) ideal decomposition, (b) approximating $E_{int}$ classically and subdividing region I into core and buffer zones [3], and (c) our proposed method, with filler region shown in gray. The schematic is not shown to scale. Red is used to indicate a MM representation, while blue indicates a QM representation. Gray filler atoms are represented with either QM or MM depending on the representation of region I. (For interpretation of the references to color in this figure legend, the reader is referred to the web version of this article.)

As a result, buffer atoms are relaxed by physically reasonable MM forces:

$$\mathbf{F}_{\mathrm{I+II}}^{\mathrm{QM/MM}}(\mathbf{R} \in \mathrm{I}_{\mathrm{buff}}) = \mathbf{F}_{\mathrm{I+II}}^{\mathrm{MM}}(\mathbf{R} \in \mathrm{I}_{\mathrm{buff}}). \tag{10}$$

For a sufficiently large region I, this provides forces for relaxing the coupled system that are equal in quality to the forces from the component representations: MM forces from a simulation of the entire system for region II and the region I buffer, and QM forces from a simulation of region I for the core of region I. The addition of correction forces introduces work energy into the total energy calculated at each step equal to the dot product of the displacement of the core and buffer atoms in that step with the correction forces applied to them. These work terms become small as the structure relaxes. The fully relaxed atomic configuration we are interested in can thus be obtained by iteratively updating atomic positions in the core of region I and in the rest of the system using QM and MM forces, respectively.

The method described above constitutes a mechanical coupling between the atomistic QM and MM domains. Because of the correction forces introduced, the MM representation of region I does not contribute to the relaxation of atoms in this QM/MM scheme. For calculating energies (which requires taking an energy difference of two or more systems), however, this smaller MM component plays an important role. By entering the QM/MM total energy in Eq. (3) with the opposite sign as the QM representation of region I, this component ensures that the fictitious energy contribution from variance in the buffer geometry between systems comes from the difference of QM and MM representations; i.e. the error from non-identical buffer geometries appears only as a difference of energy differences.

QM/MM calculations using "vacuum clusters" are performed as we have described so far, based on the literature cited throughout the description. However, this method suffers from one critical problem: except for extremely large buffer sizes, the electronic state in the core of region I is perturbed by the presence of the vacuum surface in the QM cluster calculation. This has an effect on the quality of forces for atoms in the core.

For molecular systems where the electrons are well localized to orbitals, the edge of the quantum domain can be handled by fitting a static orbital density or by placing a "link atom" at each dangling bond after cutting between QM and MM domains [15,17]. In metals, however, the sudden drop of the electronic background potential creates a deeply penetrating change in the electronic charge density due to Friedel oscillations that destroys the core atoms' perception that they are embedded in a much larger system. Recently, Zhang et al. [5] have proposed to resolve the issue of this long-range impact on the charge density by modifying the underlying KS DFT Hamiltonian to restrict the electron density near the outer edge of region I to be "bulk-like". We take an alternative approach which does not require altering the Hamilton used for QM component calculations and can be easily implemented with any existing DFT code package; to isolate the QM core from electronic perturbations, we replace the material-vacuum interface with a material–material interface that is less electronically extreme.

We introduce a set of "filler" atoms, of the same species as the host, to fill the computational cell and eliminate the presence of the vacuum surface. This replacement of the buffer-vacuum surface with a buffer–filler atom interface removes the strong electronic perturbation and replaces it with a much weaker one. To make this approach computationally attractive, the savings in CPU time from requiring fewer atoms in the buffer zone must outweigh the cost of adding filler atoms to modify the interface. Unlike the method in Ref. [5], our method does not require changes at the level of the KS formalism (and thus changes to the DFT code,) and, therefore, can be used with any of the available DFT packages. Strategies to optimally place the filler atoms in the vacuum region are discussed in more detail in Section 2.2. The setup of this approach is shown schematically in Fig. 1(c). We note that filler atoms exist only in what were previously cluster calculations and not in the MM calculation of the entire region I + II superstructure, from which region II and buffer atom forces are drawn; i.e. filler atoms do not directly influence the forces on the buffer atoms to which they are adjacent.

In plane-wave DFT codes with periodic boundary conditions (PBC)—which are common for simulating metals—the introduction of these filler atoms creates new interfaces: the material–material interface between filler atoms and buffer atoms discussed previously, and also interfaces at the periodic boundaries of the simulation cell between filler atoms. By choosing the same filler atom geometry across the multiple calculations necessary to compute a physical energy, and by holding filler atom positions totally fixed throughout the QM/MM atomic relaxations, the energetic contributions from the filler–filler interfaces largely cancel each other when energy differences are taken. Because the geometry of region I may change during relaxation, the energies from the interface between buffer and filler atoms will not cancel as well. However, this is a concern even for any method using vacuum clusters, where the geometry of the vacuum surface also changes. The extent of filler–buffer interface cancellation can be controlled by increasing the size of region I so that buffer atoms near the filler experience less deformation.

This method is similar to an earlier approach by Woodward and Rao [6] coupling a QM domain to a LGF. Surrounding a QM-relaxed core, Woodward and Rao fill the remaining QM simulation cell with atoms relaxed by the LGF. Similarly to the method proposed here, this eliminates vacuum surfaces and replaces them with material–material interfaces. However, unlike the proposed filler atoms, all of the atoms in the QM domain of Woodward and Rao are permitted to relax. For the QM/MM coupling discussed here, the equivalent method would be to simply extend the buffer atoms to fill the entire QM periodic domain.

The method of Woodward and Rao works well when accurate forces and geometries are a key objective, and has been used to study dislocation cores [18,19] and a crack tip [12] (coupling to finite elements in the latter, rather than a LGF.) However, it does not work as well for determining accurate energetics. Because atoms right up to the edge of the QM simulation domain are permitted to relax via the long range coupling force (a LGF, finite elements, MM, etc.), any expansion or contraction of these buffer atoms due to the QM core is mirrored across the QM domain boundary, causing changes in the buffer–buffer interface. While this is still a concern with our buffer–filler interface, the problem is much less severe because the filler atoms are held fixed and do not mirror the motion of the buffer atoms they form an interface with. As a result, by using filler atoms the fictitious buffer–filler interface has better cancellation across the multiple calculations required to take an energy difference than a buffer–buffer interface.

Our scheme is summarized as follows:

1. Start with a large system suitable for MM, and decompose the system by choosing atoms for region I core and buffer.
2. Choose a geometry for filler atoms, thereby creating a new region I + filler sub-system.
3. Relax region II and the region I buffer atoms using forces from the MM calculation of the entire region I + II system while holding atoms in the region I core fixed. Then relax region I core atoms using forces from the QM calculation of region I + filler while holding buffer and filler atoms fixed.
4. Evaluate $E_{\mathrm{I+II}}^{\mathrm{QM/MM}}$ using Eq. (3) and any work done by the correction forces in the last multiscale step.
5. Check for force and/or energy convergence and return to step 3 if not converged.

These steps are modified from the existing "vacuum cluster" scheme by the inclusion of filler atoms.

In principle, there is no guarantee that such a scheme converges. Because relaxations in the core and elsewhere are made sequentially, we must check force convergence either after the MM relaxation step is complete and region II and buffer atom positions are updated, or after the QM relaxation step is complete and the core atom positions are updated. In the first case, it is possible that the MM-updated positions of buffer atoms will create QM core atom forces above the desired cutoff, and in the latter case the QM-updated positions of core atoms may create MM buffer atom forces that are too large. Such non-convergence would indicate that the MM potential is not sufficiently similar to the QM representation. Constructing a new MM potential just for the QM/MM calculation would largely defeat the purpose of such a coupling scheme. In practice, however, we have found no problems obtaining force convergence below 0.01 eV/Å with our filler atom scheme after a simple rescaling of existing EAM potentials to match the DFT lattice constant. This was the case even for complex geometries like a Σ5 grain boundary.

In the present study, the target quantities we seek to compute are binding energies between solute atoms and structural defects. We follow a convention with attractive binding defined positively, and evaluate it using four separate calculations which can be interpreted as comparing the energy of the system with the solute present at the spatial defect and the solute infinitely separated from the defect. For solute–vacancy binding we have

$$E_{\mathrm{bind}}^{X-\mathrm{vac}} = (E_{(N-1)\square} + E_{(N-1)X}) - (E_{(N-2)\square X} + E_N), \tag{11}$$

where $E_N$ is the energy of a bulk system of $N$ atoms, $E_{(N-2)\square X}$ is the bulk system with a solute, $X$, and vacancy adjacent to each other, and $E_{(N-1)\square}$ and $E_{(N-1)X}$ are the bulk system with an isolated vacancy and solute, respectively. For solute–GB binding we obtain

$$E_{\mathrm{bind}}^{X-\mathrm{GB}} = (E_{N_{\mathrm{GB}}} + E_{(N-1)X}) - (E_{(N_{\mathrm{GB}}-1)X} + E_N), \tag{12}$$

where $E_{N_{\mathrm{GB}}}$ is a system of $N_{\mathrm{GB}}$ atoms and GB structure, and $E_{(N_{\mathrm{GB}}-1)X}$ is the same system with a solute at the planar GB site.

### 2.2. Implementation

MM calculations are performed with LAMMPS [20,21] using EAM potentials for Al–Mg and Al–Pb by Mendelev et al. [22] and Landa et al. [23], respectively. By varying their measure of distance, the EAM potentials were isotropically rescaled to match DFT lattice constants. MM superstructure calculations consist of 364,500 atoms of ideal face centered cubic (FCC) Al in a periodically repeating cubic cell with side length 179.06 Å for bulk calculations; the Σ5 boundary uses two symmetric grains with a total of 720,000 atoms in a rectangular box measuring 177.83 Å × 357.03 Å × 178.91 Å with the GB lying in the $XZ$-plane. These superstructures were permitted to relax once using the rescaled EAM potential [22] without any solutes or vacancies. Then they are used with the fixed box sizes given above when site defects are introduced. Compared to smaller MM domains—each with approximately half as many atoms—these superstructures give MM binding energies which are converged to within 0.01 eV.

All QM calculations are performed using the Vienna *Ab initio* Simulation Package (VASP) [24–27] plane-wave DFT code. Since we perform size convergence tests up to very large numbers of atoms, we use simple ultra-soft pseudopotentials (US PP) [28,29] from the standard VASP library with the local density approximation exchange–correlation functional [30]. We use a plane wave basis set with an energy cut-off of 200 eV and Methfessel–Paxton smearing [31] with a width of 0.1 eV.

Periodic DFT results use $k$-meshes with at least 32,000 $k$-points per reciprocal atom (KPPRA). This gives well converged energies and converges the unit cell lattice constant on the order of 1 mÅ,

which is <0.03% of the 3.98 Å lattice constant found for the USPP for Al. This provides a precise target for rescaling EAM potentials.

Size convergence for periodic DFT calculations and for the size of region I in QM/MM calculations is shown explicitly in the plots of Section 3. For vacuum clusters, an inter-cluster vacuum distance of 10 Å was found to be sufficient to decouple the cluster from its periodic images. Since the vacuum clusters are aperiodic to a good approximation, we use only a single *k*-point, the Gamma point, in those calculations.

Our general scheme for QM/MM coupling is described in Section 2.1 and a detailed description of the implementation can be found in Appendix A, but it is important to discuss some details of the geometry of the method.

Construction of region I is performed by choosing a small number of "seed" atoms around which concentric shells of neighboring atoms are built, together making up core and buffer layers. In the calculations using bulk geometry, we always use two seed atoms: one at which we may place the solute, and the other at which we may place a vacancy, as shown in Fig. 2(a). For calculations using the GB geometry, we use only the GB site of interest, see Fig. 2 (b). Constructing region I by forming concentric shells keeps these locations of most interest as far from the outside edge of region I as possible. For the QM/MM method with vacuum clusters, we place the clusters in a rectangular prism cell with 10 Å between the extremal atoms of the clusters and the closest atoms in the periodic images.

For our improved QM/MM method with filler atoms, we have a great deal of freedom in how we might choose the position of filler atoms. In the spirit of isolating the core of region I as best as possible, we choose the positions of filler atoms from among the initial position of atoms in region II such that a rectangular prism encasing region I has empty space filled, as shown in Fig. 2 for both bulk and GB geometries. Since region II is not periodic in this small box, this method creates six filler–filler interfaces on the sides of our rectangular prism where we have forced periodicity, with a minimum distance of 2.7 Å (1.4 Å) between filler atoms and the closest filler atom in a periodic image cell for bulk (GB) geometry. At the interface between the filler and buffer zones there is, initially, no imperfection. As the QM/MM system relaxes these filler atoms are held fixed and no longer correspond to the positions of atoms in region II, so a small interface also develops between buffer and filler atoms. Because the interface between the buffer and filler atoms is due to the relaxation of the buffer from its initial position, its severity can be controlled by the size of region I and we can expect it to be less extreme than the interfaces at the cell boundaries and much less extreme than the vacuum surface of the original method.

Because our test systems can be simulated using regular periodic DFT, we could in principle have chosen filler atom positions very carefully to eliminate any filler–filler interface. Since the true interest of QM/MM methods is to push beyond systems which can be simulated by DFT alone, we have avoided this. Our method for constructing region I and the filler geometry is completely general, and results in imperfections on all six faces of the QM simulation domain. Therefore, our comparison between QM/MM and fully periodic DFT results provides and accurate estimate of the performance that can be expected in novel geometries not obtainable with periodic DFT.

## 3. Results

### 3.1. MM/MM results

We rely on the MM domain to provide accurate positions for the buffer atoms and to capture the long range elastic behavior of the system. To probe the effect of structural and elastic mismatch between the QM and MM representations systematically, we replace the QM calculation with another MM calculation and implement a MM/MM coupling. By using a different potential or the same potential with a different lattice constant for the QM-replacement than we use for the regular MM domain, we can systematically vary the degree of structural and elastic disagreement between the two representations and observe the effect on the energetics.

To this end, we must first establish the sensitivity of the bulk moduli of the two EAM potentials to the scaling of their lattice parameters. Fig. 3 shows that the moduli vary by less than ±8% for lattice constant variations of ±2%. We can also see that, when scaled to match the DFT lattice constant, both potentials slightly underestimate the DFT value of the bulk modulus. Because the bulk modulus responds differently to lattice rescaling for the two potentials used, we are able to isolate the effect of bulk moduli differences with the same lattice constant in MM/MM coupling. For elastic mismatches on the order of 2 GPa—the difference between DFT and the Mendelev potential used in full QM/MM calculations—the impact on binding energies is small, with the largest changes lying between 0.005 eV and 0.02 eV depending on the system.

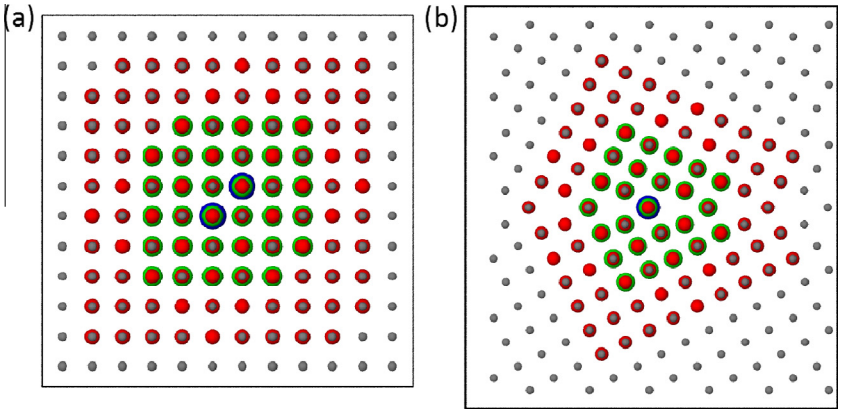


**Fig. 2.** Region I + filler atomic structures for (a) bulk structure and (b) Σ5 GB each with two core shells and two buffer shells looking down the *c*-axis, which is the axis of rotation for the GB. Seed atoms are shown large in blue, the remaining core atoms are shown medium in green, the two buffer shells are shown small in red, and all filler atoms are shown very small in gray. Black boxes indicate the periodic domain. Visualised using Ovito [32]. (For interpretation of the references to color in this figure legend, the reader is referred to the web version of this article.)

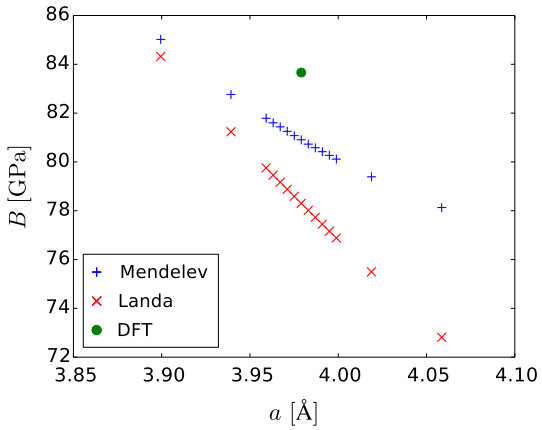


**Fig. 3.** Bulk moduli for the two EAM potentials of Mendelev [22] (blue +) and Landa [23] (red ×) scaled to various lattice constants, and the USPP DFT result (green ○). (For interpretation of the references to color in this figure legend, the reader is referred to the web version of this article.)

We can also investigate the combined effect of lattice and moduli mismatches on binding energies by using differently scaled potentials. Fig. 4 shows the binding energies as the QM-replacement potential is rescaled to lattice constants of ±1% while the MM potential is held fixed at the reference scaling that matches the DFT lattice value. Results are shown for several sizes of region I; while the system with the largest choice of region I tends to show the weakest dependence on lattice mismatch, the effect is small and all three choices give very similar results. This rapid convergence with respect to the size of region I should not be expected in full QM/MM calculations, where electronic perturbations can have an impact on length scales larger than the EAM cutoff distance used in these simpler MM/MM calculations. Across all four combinations of solute and defect, the response to strain is smooth. In general we see a much stronger sensitivity to lattice constant mismatch for Pb than for Mg, with relative energy errors for Pb of order 15% at a strain of 1%. For QM/MM calculations, EAM potentials are rescaled to exactly match DFT lattice constants, thus we expect very little error for the bulk geometry. For the case of the GB, the EAM potential does not yield the exact same GB structure as the DFT and we expect mismatch effects to be more significant.

### 3.2. QM/MM results

Before performing a full set of QM/MM calculations of binding energies, we first assess whether the electronic perturbations at the interfaces are indeed mitigated by the use of filler atoms. To this end, we examined the maximum initial forces for the QM component of the perfect bulk, $F^0_{\max}$, shown in Fig. 5 plotted against the number of atoms in the QM component calculation, $N_{\mathrm{QM}}$. Since we simulate the perfect bulk, the forces should ideally be zero, although we see this is not the case. When using vacuum clusters, the vacuum surface perturbs forces in the QM core, while the calculations using filler atoms experience a smaller perturbation from the filler–filler interfaces at the periodic boundaries. For both the red filler atom and blue vacuum cluster series in Fig. 5, the leftmost data point corresponds to a system with two shells of core atoms and one shell of buffer atoms; each further point adds a buffer shell.

We can see that the filler atom method provides a much higher quality of forces, and even the smallest filler atom calculation (450 atoms) out-performs the largest vacuum cluster (1584 atoms) examined. These results are qualitatively consistent with other QM multiscale schemes: Choly et al. [1] report a maximum initial force of 0.45 eV/Å using a 32-atom vacuum cluster for the QM calculation (in which all atoms belong to the QM core, i.e. no buffer atoms,) and Nair et al. [12] report a maximum initial force slightly below 0.01 eV/Å in the QM core of a calculation with 452 atoms and no vacuum surface (using the method of Woodward and Rao

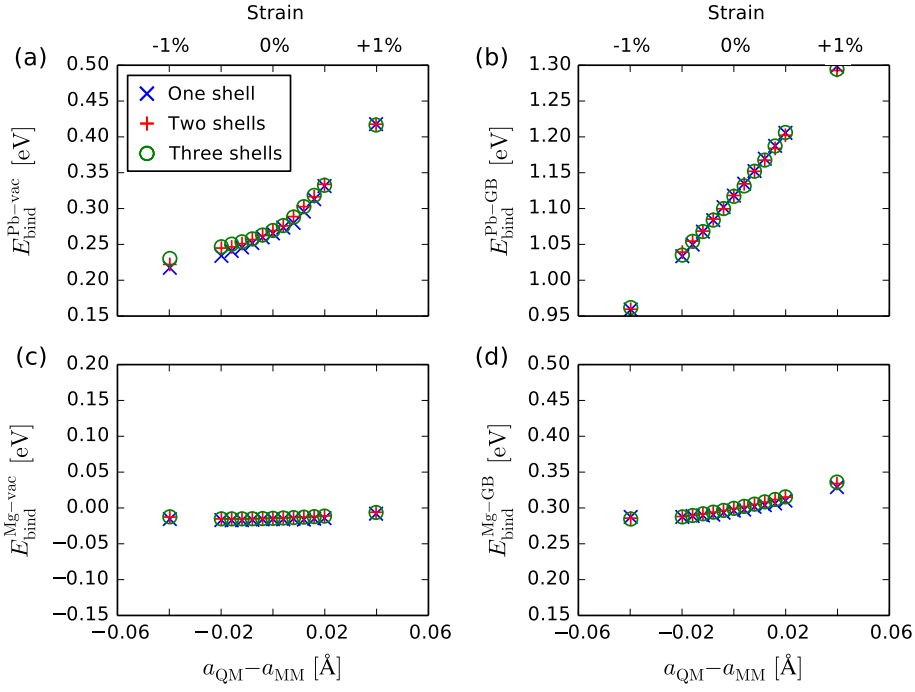


**Fig. 4.** Solute–vacancy and solute–GB binding energies with MM/MM coupling as a function of the lattice mismatch between the QM-replacement potential and the regular MM potential. Two core shells are used, and one, two, and three buffer shells are used for blue ×, red +, and green ○, respectively. Results are shown for Pb (a and b) and Mg (c and d) binding to a vacancy (a and c) and a GB site (b and d). (For interpretation of the references to color in this figure legend, the reader is referred to the web version of this article.)

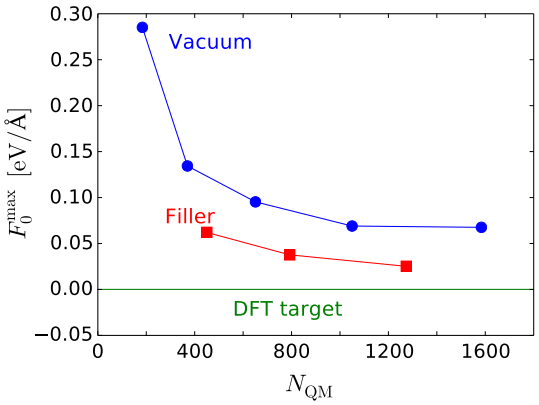


**Fig. 5.** Largest QM/MM initial force for bulk Al system using vacuum cluster (blue ○) and filler atom method (red □). Desired bulk force, 0 eV/Å, is shown in green. Results are plotted against the number of atoms in used for the QM calculation. (For interpretation of the references to color in this figure legend, the reader is referred to the web version of this article.)

similar to our filler atom calculations). The moderately better performance-per-atom achieved by Nair et al. [12] may be attributed to the fact that they maintain regular DFT periodicity in one dimension, while we break periodicity in all three dimensions.

However, the improved quality of using filler atoms comes at a cost: filler atom calculations are more expensive than their vacuum cluster counterparts with the same number of atoms in region I because they require a $k$-mesh grid with more than a single point and carry the extra cost for adding filler atoms. Since we want a method that is not only accurate, but also efficient, it is important to be able to compare the computational cost of our QM/MM calculations. Because the overhead for coupling is minimal, and we begin with a MM relaxed superstructure so that the MM calculations only need to accommodate strains from relaxation in the small QM core, the cost of the QM component calculations completely dominates the total computational effort. The cost of plane-wave DFT calculations scales roughly with the third power of the number of electrons (which is proportional to the third power of the number of atoms, $N_{\mathrm{QM}}$, in systems made up mostly of one species) and linearly with the number of irreducible $k$-points, $n_k$. The total cost for a calculation can thus be estimated as

$$\mathrm{Cost} \approx N_{\mathrm{QM}}^3 \times n_k \times n_{\mathrm{ec}}, \tag{13}$$

where $n_{\mathrm{ec}}$ is the total number of electronic cycles the calculation uses. Calculations which are electronically more complex or which require multiple iterations of ionic relaxation will have a larger value of $n_{\mathrm{ec}}$ than those which are simple or already close to their relaxed state. This approximation correlates linearly with CPU time and is independent of the hardware on which the calculation is performed. We use this formula to compare the total cost of different calculations, rescaled by the cost for a four-atom unit cell of Al with good lattice parameters that requires only electronic convergence.

To see the aggregate effect of all the sources of error (intrinsic representation error, differences in structural and elastic representation, and fictitious electronic forces), we have performed a series of fully coupled QM/MM calculations with both the vacuum cluster method and the improved filler atom method. The comparison of these results to periodic DFT results is shown in Fig. 6 plotted against our estimated computational cost from Eq. (13) normalized by the unit cell cost. As in Fig. 5, the leftmost data point for the vacuum cluster and filler calculations have two core shells of atoms and one buffer shell, with an extra buffer shell being added at each further data point; detailed run parameters can be found in Tables 1–3. We have also included a band of ±0.03 eV about the best-converged periodic results as a suggestion for the window of results which are of high quality.

For Mg-vacancy and Pb-GB binding energies, the vacuum cluster and the filler method give comparable results: at similar computational cost, both QM/MM methods agree well with periodic DFT results and, importantly, neither display large changes

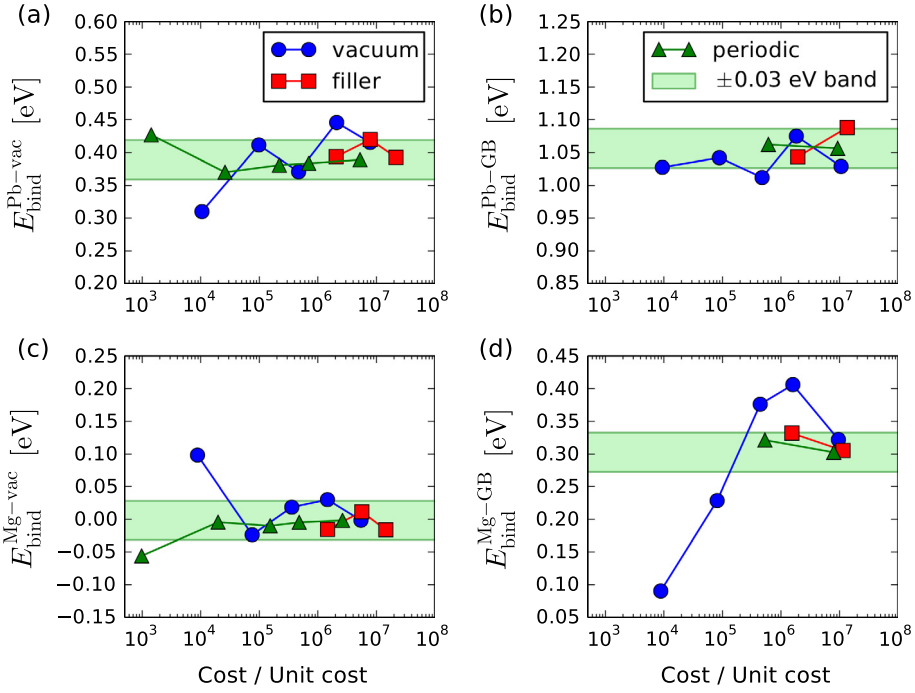


**Fig. 6.** Solute–vacancy and solute–GB binding energies for QM/MM coupling with vacuum clusters (blue ○), QM/MM coupling with filler atoms (red □), and regular periodic DFT (green △), plotted against a normalized estimate of the calculation cost. The green band of ±0.03 eV is centered about the best converged periodic result. Results are shown for Pb (a and b) and Mg (c and d) binding to a vacancy (a and c) and a GB site (b and d). (For interpretation of the references to color in this figure legend, the reader is referred to the web version of this article.)

**Table 1**
Periodic DFT binding energies. Run parameters given for GB binding are for the GB component calculations. System sizes, $L_x, L_y, L_z$ are for relaxed pure systems (i.e. no solutes or vacancies).

| System | Atoms | $L_x, L_y, L_z$ (Å) | $k$-mesh | Binding (eV) |
|---|---|---|---|---|
| Pb-vacancy | 32 | 8.0, 8.0, 8.0 | $10 \times 10 \times 10$ | 0.42 |
| Pb-vacancy | 108 | 11.9, 11.9, 11.9 | $7 \times 7 \times 7$ | 0.37 |
| Pb-vacancy | 256 | 15.9, 15.9, 15.9 | $5 \times 5 \times 5$ | 0.38 |
| Pb-vacancy | 500 | 19.9, 19.9, 19.9 | $4 \times 4 \times 4$ | 0.38 |
| Pb-vacancy | 864 | 23.9, 23.9, 23.9 | $4 \times 4 \times 4$ | 0.39 |
| Mg-vacancy | 32 | 8.0, 8.0, 8.0 | $1 \times 3 \times 5$ | −0.06 |
| Mg-vacancy | 108 | 11.9, 11.9, 11.9 | $7 \times 7 \times 7$ | −0.00 |
| Mg-vacancy | 256 | 15.9, 15.9, 15.9 | $5 \times 5 \times 5$ | −0.01 |
| Mg-vacancy | 500 | 19.9, 19.9, 19.9 | $4 \times 4 \times 4$ | −0.00 |
| Mg-vacancy | 864 | 23.9, 23.9, 23.9 | $4 \times 4 \times 4$ | −0.00 |
| Pb-GB | 400 | 17.7, 45.6, 7.9 | $4 \times 2 \times 10$ | 1.06 |
| Pb-GB | 1080 | 26.6, 54.4, 11.9 | $3 \times 2 \times 5$ | 1.06 |
| Mg-GB | 400 | 17.7, 45.6, 7.9 | $4 \times 2 \times 10$ | 0.32 |
| Mg-GB | 1080 | 26.6, 54.4, 11.9 | $3 \times 2 \times 5$ | 0.30 |

**Table 2**
QM/MM binding energies using vacuum clusters. Run parameters given for GB binding are for the GB component calculations.

| System | QM atoms | Buffer shells | $k$-mesh | Binding (eV) |
|---|---|---|---|---|
| Pb-vacancy | 184 | 1 | $1 \times 1 \times 1$ | 0.31 |
| Pb-vacancy | 370 | 2 | $1 \times 1 \times 1$ | 0.41 |
| Pb-vacancy | 651 | 3 | $1 \times 1 \times 1$ | 0.37 |
| Pb-vacancy | 1050 | 4 | $1 \times 1 \times 1$ | 0.45 |
| Pb-vacancy | 1584 | 5 | $1 \times 1 \times 1$ | 0.42 |
| Mg-vacancy | 184 | 1 | $1 \times 1 \times 1$ | 0.10 |
| Mg-vacancy | 370 | 2 | $1 \times 1 \times 1$ | −0.02 |
| Mg-vacancy | 651 | 3 | $1 \times 1 \times 1$ | 0.02 |
| Mg-vacancy | 1050 | 4 | $1 \times 1 \times 1$ | 0.03 |
| Mg-vacancy | 1584 | 5 | $1 \times 1 \times 1$ | −0.00 |
| Pb-GB | 147 | 1 | $1 \times 1 \times 1$ | 1.03 |
| Pb-GB | 309 | 2 | $1 \times 1 \times 1$ | 1.04 |
| Pb-GB | 561 | 3 | $1 \times 1 \times 1$ | 1.01 |
| Pb-GB | 923 | 4 | $1 \times 1 \times 1$ | 1.07 |
| Pb-GB | 1415 | 5 | $1 \times 1 \times 1$ | 1.03 |
| Mg-GB | 147 | 1 | $1 \times 1 \times 1$ | 0.09 |
| Mg-GB | 309 | 2 | $1 \times 1 \times 1$ | 0.23 |
| Mg-GB | 561 | 3 | $1 \times 1 \times 1$ | 0.38 |
| Mg-GB | 923 | 4 | $1 \times 1 \times 1$ | 0.41 |
| Mg-GB | 1415 | 5 | $1 \times 1 \times 1$ | 0.32 |

**Table 3**
QM/MM binding energies using filler atoms. Run parameters given for GB binding are for the GB component calculations.

| System | QM atoms | Buffer shells | $k$-mesh | Binding (eV) |
|---|---|---|---|---|
| Pb-vacancy | 450 | 1 | $4 \times 4 \times 5$ | 0.39 |
| Pb-vacancy | 792 | 2 | $4 \times 4 \times 4$ | 0.42 |
| Pb-vacancy | 1274 | 3 | $3 \times 3 \times 3$ | 0.39 |
| Mg-vacancy | 450 | 1 | $4 \times 4 \times 5$ | −0.02 |
| Mg-vacancy | 792 | 2 | $4 \times 4 \times 4$ | 0.01 |
| Mg-vacancy | 1274 | 3 | $3 \times 3 \times 3$ | −0.02 |
| Pb-GB | 517 | 1 | $4 \times 4 \times 4$ | 1.04 |
| Pb-GB | 991 | 2 | $3 \times 3 \times 4$ | 1.09 |
| Mg-GB | 517 | 1 | $4 \times 4 \times 4$ | 0.33 |
| Mg-GB | 991 | 2 | $3 \times 3 \times 4$ | 0.31 |

in energy with respect to increasing system size. In contrast, for Pb-vacancy and Mg-GB binding energies, the filler method provides much more reliable results. At the first point of overlapping cost for Pb-vacancy binding (i.e. at a rescaled cost of $\approx 1.5 \times 10^6$), the vacuum cluster calculation returns an energy that deviates by nearly 0.06 eV from the periodic DFT value—twice the deviation of the worst-performing filler method calculation across all four binding energies. Further, the vacuum cluster results for this system appear to be drifting upwards with increasing system size, so while the largest calculation performed lies within the $\pm 0.03$ eV band it is possible that a larger calculation would again return a result further from the desired value. For Mg-GB binding, the vacuum cluster method gives absolutely no indication of being converged with respect to size, with an energy change of 0.08 eV—more than 25% of the total binding energy—between the two largest calculations.

The filler atom calculations give results which are consistently well grouped within 0.04 eV of each other with respect to increasing system size. Moreover, while sometimes overestimating and other times underestimating the benchmark result, the filler atom method always gives values within $\pm 0.03$ eV of the best periodic DFT result. In comparison, the vacuum clusters sometimes yield good results—e.g. Mg-vacancy binding—but at other times the results are poor, lying farther from the periodic DFT value or failing to indicate convergence. Using the smallest QM domain, filler atom QM/MM calculations yield more reliable results than vacuum cluster QM/MM calculations of similar computational cost.

Our work can be compared to the work of Zhang et al. [5], which resolves the problem of vacuum surface perturbations by modifying the KS DFT Hamiltonian to constrain the electron density to be bulk-like and is the only other state-of-the-art QM/MM scheme to address this issue successfully. The energetic tests presented by Zhang et al. include the vacancy formation energy in bulk Al, for which their scheme differs from the periodic DFT calculations by 0.04 eV. Similarly, for the chemisorption of CO on a Pd surface, the binding energy to the surface differs from the periodic DFT benchmark by 0.02 eV. These values are comparable to the level of agreement in the present work, and are on the same order as inherent differences in energy due to the exchange–correlation approximation in DFT, i.e. their method was successful. Among the other tests of Zhang et al. is an investigation of the magnetic moment of Fe. In this they demonstrate that their constrained density approach handles magnetic systems well. It would be of interest to perform similar tests on magnetic systems with our scheme, which would rely on the magnetic perturbations from filler–filler and filler–buffer interfaces decaying at a comparable speed as the electron density perturbations. While Zhang et al. do not explicitly report the computational cost of their method, the QM domains used in the previously mentioned tests contain somewhat fewer atoms than our smallest filler atom calculations, thus we expect their method to be more cost effective. However, their method is less straightforward to port to different QM codes since it involves a change in the KS formalism. It is also not obvious how the method of Zhang et al. handles complex systems with defects running through the QM/MM interface (e.g. GBs, which were the motivation for developing the present methodology)—in such systems a bulk-like charge constraint may not work well when applied to non-bulk-like atoms.

## 4. Conclusions

We have developed an improved method for QM/MM coupling for metallic systems that uses extra filler material surrounding the QM region to reduce the undesirable influence of fictitious electronic perturbations on forces and energies in the QM core. In combination with buffer atoms [3], our method provides high quality QM energetics for systems that could not be calculated by DFT alone and can be straightforwardly implemented using any existing QM or MM code. The addition of filler material may be useful for other QM multiscale schemes which currently utilize DFT vacuum clusters; here we have explored only one possible implementation of this general principle.

A particular novelty to the approach presented here is its easy applicability to structures in which a defect (e.g. GB) passes

through the coupling domain. This was a driving motivation for choosing to couple the QM domain to a larger MM system instead of some other representation of the far field. For simple metals, EAM potentials offer a powerful tool to capture the elastic nonlinearities in the defect structure. However, these EAM potentials do not contain any directionally dependent terms and do not capture the strongly directional bonding that may be important in some metals, e.g. Nb or Mo. This is in general a limitation for QM/MM coupling, and the method presented here is not immune to it.

To test the computational efficiency of the proposed approach we considered FCC Al as a host system and calculated the binding energies of Mg and Pb to both vacancies and to a symmetric Σ5 GB at the site lying in the GB plane. By replacing the QM calculation with another MM calculation that uses a different MM potential, we provided estimates for the effect of lattice and elastic mismatch between the two domains on these binding energies. While errors due to mismatched elastic properties remain small, our analysis shows that it is important to use empirical potentials that provide a good description of the geometry.

By studying the initial forces in a fully coupled QM/MM calculation of bulk material, where all forces should be zero, we demonstrated that our improved filler atom method gives much higher quality forces for systems with far fewer atoms than the vacuum cluster method. While the filler atoms add to the cost of the calculation, we found that the quality of binding energies was superior to the vacuum cluster calculations when costs are similar. QM/MM filler atom results for all sizes of QM domain studied lie within 0.04 eV of each other. This is not the case for QM/MM calculations that use vacuum clusters, where results can vary widely and, in a number of cases, do not show clear evidence of converging, even at large system sizes. Further, all of the filler atom QM/MM results agree within ±0.03 eV with periodic DFT results for the same system. In conclusion, we expect this approach to provide a robust starting point for studies of low-symmetry defect structures. A prominent example that this approach could be applied to is arbitrarily misoriented GBs, which have so far been inaccessible to *ab initio* calculations.

## Acknowledgements

LH was supported by an Alexander Graham Bell Post-Graduate Scholarship from the Natural Sciences and Engineering Research Council of Canada (NSERC). LH would also like to thank MagNET [33] for providing funds to visit the Max-Planck-Institut für Eisenforschung. The authors would also like to acknowledge WestGrid/Compute Canada for providing computational resources. This project has received funding from the European Research Council (ERC) under the European Unions Horizon 2020 research and innovation programme (Grant Agreement No. 639211).

## Appendix A. QM/MM implementation details

Since the elastic coupling between the QM and MM domains is mediated by the motion of atoms in region I, coupling can be achieved without modifying the QM or MM codes, and the details of coupling described here may be implemented in any general scripting language and can make use of any QM and MM codes which will perform energy minimization and output atomic positions and forces.

To partition the system, we begin with a large MM-relaxed superstructure and select one or more atoms of interest, called "seed" atoms, which we would like to place in the very center of region I. Using a cut-off distance, $d_{\text{cut}}$, we then search the superstructure for all other atoms within $d_{\text{cut}}$ of the seed atoms. The atoms found form the first "shell" of region I core. This process is repeated until a desired number of shells for the core and buffer zones have been found. We have used $d_{\text{cut}} = 3.0$ Å, which is slightly larger than the first nearest neighbor (1NN) distance of 2.81 Å. We found that the resulting region I structures were insensitive to the choice of $d_{\text{cut}}$ in most of the range between the 1NN distance and the lattice constant—even in the more complex GB case. Geometries with two core and two buffer shells for bulk and GB structures are shown in the body of the text in Fig. 2.

While it is possible to construct filler material in many ways, we chose to use the initial positions of atoms in region II. This was done by calculating a bounding box around region I, padding it with 3.0 Å, and choosing as filler all the atoms inside the box that are not already region I atoms. After calculating a new bounding box for the region I + filler atoms, we add 2.7 Å (1.4 Å) between the outer filler atoms and the next periodic cell for the bulk (GB) structure. This introduces six filler-filler interfaces, one on each side of the rectangular prism making up the region I + filler simulation domain. With this choice, there is initially no interface between the filler and buffer atoms.

In principle, this method works with any alloy composition in region II for which a suitable classical potential exists, but in practice our implementation uses a pure host material. To perform calculations with solute atoms, the chemistry of region I + filler is changed only in the QM representation. Provided that the size of the core of region I is comparable to or greater than the cut-off radius of the classical potential being used, the forces and energies from the MM components of the QM/MM calculation are still valid since their energetic contributions from the atom(s) which we have replaced with a host atom(s) will cancel out and the buffer atoms will be too far away to feel any erroneous forces.

As the coupled system relaxes and buffer atom positions are updated using MM forces from the entire superstructure, an interface develops between the buffer and filler atoms. Since filler atoms do not exist in the calculation of the superstructure, it is possible for region I to drift relative to the fixed filler as it relaxes. To prevent such drift from causing excessively large buffer–filler interfacial energies, the atoms of region I are re-centered in their filler atom cage at each coupled step.

The detailed steps of our algorithm are as follows:

1. Choose (and rescale if necessary) a classical potential to match the QM lattice structure and elastic properties as well as possible.
2. Relax a superstructure using this potential.
3. Choose a small number of (adjacent) atoms to form the seed of region I.
4. Build atomic shells around these seeds until the desired number of core and buffer shells is reached. These atoms are region I, all other atoms are region II.
5. Build a bounding box around region I atoms, pad it, and search for filler atoms among the initial positions of the atoms in region II.
6. Write the necessary input for your component QM and MM simulations, e.g. structure files, potentials, etc. Any vacancies should be deleted from both QM and MM structure files, but solute atoms will have their true species only in the QM simulation.
7. Perform a static MM calculation of region I + filler and store $\mathbf{F}^{\text{MM}}(\mathbf{R} \in \text{I}_{\text{buff}})$ for later use in $\mathbf{F}^{\text{corr}}_{\text{I}_{\text{buff}}}$.
8. Relax region II and region I buffer using a MM calculation of the entire system with atoms in the region I core held fixed. Store the initial values of $\mathbf{F}^{\text{MM}}_{\text{I}}(\mathbf{R} \in \text{I}_{\text{core}})$ for later use in $\mathbf{F}^{\text{corr}}_{\text{I}_{\text{core}}}$. In the first coupled step, the relaxation here is skipped since the structure is already MM relaxed.

9. Using the updated buffer atom positions, relax the region I core using a QM calculation of region I + filler with the buffer and filler atoms held fixed. Store the initial values of $\mathbf{F}_{\mathrm{I}}^{\mathrm{QM}}(\mathbf{R} \in \mathrm{I}_{\mathrm{core}})$ and $\mathbf{F}_{\mathrm{I}}^{\mathrm{QM}}(\mathbf{R} \in \mathrm{I}_{\mathrm{buff}})$ for use in $\mathbf{F}_{\mathrm{I}_{\mathrm{core}}}^{\mathrm{corr}}$ and $\mathbf{F}_{\mathrm{I}_{\mathrm{buff}}}^{\mathrm{corr}}$, respectively. Store the largest force in the core.
10. With updated core positions, perform static MM calculations of region I + II and region I + filler.
11. Using the final energy from the QM calculation, the two MM energies from step (10), and approximating the work terms using the stored forces and core and buffer atom displacements, calculate the total energy.
12. Using the largest force from region II or buffer from the static MM evaluation of region I + II, check for force convergence. (The QM forces in the core are converged already, since we have run a relaxation there. MM forces in region II and buffer *were* converged, but the updated core atom positions will change forces, particularly on the buffer atoms.)
13. If not converged, return to step (7) and repeat.
14. Take the energy difference of two or more QM/MM calculations to find a desired physical energy.

The computational overhead for the coupling is typically small and calculation cost is dominated by the cost of the QM region I + filler calculation.

## References

[1] N. Choly, G. Lu, E. Weinan, E. Kaxiras, Phys. Rev. B 71 (2005) 094101.
[2] X. Zhang, G. Lu, Phys. Rev. B 76 (2007) 245111.
[3] Y. Liu, G. Lu, Z. Chen, N. Kioussis, Modell. Simul. Mater. Sci. Eng. 15 (2007) 275.
[4] Y. Zhao, C. Wang, Q. Peng, G. Lu, Comput. Mater. Sci. 50 (2010) 714.
[5] X. Zhang, G. Lu, W. Curtin, Phys. Rev. B 87 (2013) 054113.
[6] C. Woodward, S. Rao, Phys. Rev. Lett. 88 (2002) 216402.
[7] M. Ghazisaeidi, D. Trinkle, Phys. Rev. B 82 (2010) 064115.
[8] J.Q. Broughton, F.F. Abraham, N. Bernstein, E. Kaxiras, Phys. Rev. B 60 (1999) 2391.
[9] S. Ogata, E. Lidorikis, F. Shimojo, A. Nakano, P. Vashishta, R.K. Kalia, Comput. Phys. Commun. 138 (2001) 143.
[10] L. Shilkrot, R.E. Miller, W.A. Curtin, J. Mech. Phys. Solids 52 (2004) 755.
[11] G. Lu, E.B. Tadmor, E. Kaxiras, Phys. Rev. B 73 (2006) 024108.
[12] A. Nair, D. Warner, R. Hennig, W. Curtin, Scripta Mater. 63 (2010) 1212.
[13] S. Dapprich, I. Komáromi, K.S. Byun, K. Morokuma, M.J. Frisch, J. Mol. Struct. (Thoechem) 461 (1999) 1.
[14] T. Vreven, K. Morokuma, Ö. Farkas, H.B. Schlegel, M.J. Frisch, J. Comput. Chem. 24 (2003) 760.
[15] T. Vreven, K.S. Byun, I. Komáromi, S. Dapprich, J.A. Montgomery, K. Morokuma, M.J. Frisch, J. Chem. Theory Comput. 2 (2006) 815.
[16] N. Govind, Y. Wang, A. Da Silva, E. Carter, Chem. Phys. Lett. 295 (1998) 129.
[17] N. Bernstein, J.R. Kermode, G. Csanyi, Rep. Prog. Phys. 72 (2009) 026501.
[18] C. Woodward, Mater. Sci. Eng.: A 400 (2005) 59.
[19] M. Ghazisaeidi, D. Trinkle, Acta Mater. 60 (2012) 1287.
[20] S. Plimpton, J. Comput. Phys. 117 (1995) 1.
[21] http://lammps.sandia.gov.
[22] M. Mendelev, M. Asta, M. Rahman, J. Hoyt, Phil. Mag. 89 (2009) 3269.
[23] A. Landa, P. Wynblatt, D. Siegel, J. Adams, O. Mryasov, X.-Y. Liu, Acta Mater. 48 (2000) 1753.
[24] G. Kresse, J. Hafner, Phys. Rev. B 47 (1993) 558.
[25] G. Kresse, J. Hafner, Phys. Rev. B 49 (1994) 14251.
[26] G. Kresse, J. Furthmüller, Comput. Mater. Sci. 6 (1996) 15.
[27] G. Kresse, J. Furthmüller, Phys. Rev. B 54 (1996) 11169.
[28] D. Vanderbilt, Phys. Rev. B 41 (1990) 7892.
[29] G. Kresse, J. Hafner, J. Phys.: Condens. Matter 6 (1994) 8245.
[30] J.P. Perdew, A. Zunger, Phys. Rev. B 23 (1981) 5048.
[31] M. Methfessel, A. Paxton, Phys. Rev. B 40 (1989) 3616.
[32] A. Stukowski, Modell. Simul. Mater. Sci. Eng. 18 (2010) 015012.
[33] http://www.magnet.ubc.ca.